pdftitle= J(O ^{1}D) at Cape Grim 2000 - 2005
pdfauthor=S.R. Wilson
title Manuscript prepared for J. Name
with version 4.1 of the LaTeX class copernicus_discussions.cls.
Date: 28 October 2014

Characterisation of *J(O ^{1}D)* at Cape Grim 2000 - 2005

S.R. Wilson[1]

[1]Centre for Atmospheric Chemistry, School of Chemistry, University of Wollongong, NSW, Australia

Correspondence to: Stephen Wilson
(swilson@uow.edu.au)

Abstract

abstr Estimates of the rate of production of excited oxygen atoms due to the photolysis of ozone $J(\mathrm{O}^1D)$ have been derived from radiation measurements carried out at Cape Grim, Tasmania (40.6S, 144.7E). The measurements have a total uncertainty of ¡ 25 %. The photolysis estimates agree well with model estimates of clear sky photolysis rates. Observations spanning 2000 - 2005 have been used to quantify the impact of season, clouds and ozone column amount. The annual cycle of $J(\mathrm{O}^1D)$ has been investigated via monthly means. These means show an inter-annual variation (monthly standard deviation) of 9%, but in midsummer and midwinter this reduces to 3 - 4%. Variations in solar zenith angle and total oxone column explain 86% of the observed signal variation of the individual measurements. The impact of total column ozone, expressed as a Radiation Amplification Factor (RAF), is found to be $\sim$1.43, in agreement with model estimates. This ozone dependence explains 20% of the variation observed at medium solar zenith angles (30 - 50°). The impact of clouds results in a median reduction of 22% in $J(\mathrm{O}^1D)$ for the same solar zenith angle range. At all solar zenith angles less than 50° approximately 1% of measurements show enhanced $J(\mathrm{O}^1D)$ as determined by comparisons with a clear sky model. Apparently due to cloud scattering and this fraction climbs to 25% at larger solar zenith angles. Including estimates of cloudiness derived from Long Wave Radiation measurements resulted in a statistically significant fit to observations but the quality of the fit did not increase significantly as measured by the adjusted R^2.

1 Introduction

introIt is widely recognised that the chemistry of the clean troposphere is driven by a few key oxidizing species, with a major contributor being the hydroxyl radical (OH) (Crutzen, 1974). The hydroxyl radical reacts rapidly with a wide range of compounds, including methane, CO, and hydrocarbons. The concentration of OH present in the atmosphere is always small, but because of its high reactivity it can still play a dominant role in determining the atmospheric fate of organics. It has also long been realised that changes in the amount of OH in the atmosphere

could have a profound effect on global air quality and there has been a long-term effort to develop techniques to measure the key chemical species (Heard and Pilling, 2003). The most direct measure is the concentration of OH itself. There are several techniques now in use for such measurements, including fluorescence, UV absorption and mass spectrometry (Heard and Pilling, 2003) although only one long term measurement set has been reported to our knowledge (Rohrer and Berresheim, 2006).

The primary source of OH is through the photolysis of ozone to produce $\mathrm{O}(^1D)$ through the reactions:

$$\mathrm{O_3} + h\nu \xrightarrow{J(\mathrm{O}^1D)} \mathrm{O}(^1D) + \mathrm{O_2}\left(^1\Delta_g, ^3\Sigma_g^-\right) \quad \text{(R1)}$$

$$\mathrm{O}(^1D) + \mathrm{H_2O} \xrightarrow{k_3} 2OH \quad \text{(R2)}$$

$$\mathrm{O}(^1D) + M \xrightarrow{k_2} O(^3P) \quad \text{(R3)}$$

The fraction of $\mathrm{O}(^1D)$ reacting with water (and hence producing OH) (Q) is given by:

$$Q = k_3[H_2O]/(\, k_3[H_2O] + \sum_i k_i[M_i]) \quad (1)$$

Here the summation is over the collision partners M_i, primarily $\mathrm{O_2}$ and $\mathrm{N_2}$. Q depends on the amount of water vapour, but typically around 10% of $\mathrm{O}(^1D)$ produced reacts to form OH ($Q \approx 0.1$). This can be calculated provided atmospheric pressure and the water vapour concentration is known, since the rate constants have been measured (Sander et al., 2006).

The rate of ozone photolysis in reaction (1), $J(\mathrm{O}^1D)$, can be described by:

$$J(\mathrm{O}^1D) = \int \sigma(\lambda,T)\phi(\lambda,T)F(\lambda)d\lambda \quad (2)$$

which is the wavelength integration of $\sigma(\lambda,T)$, the (temperature dependent) absorption cross-section of ozone, $\phi(\lambda,T)$, the quantum yield of $\mathrm{O}(^1D)$ production, and $F(\lambda)$, the "spectral

actinic flux density", which is the spherically integrated spectral radiance. There are a number of measurements of $J(O^1D)$ via chemical actinometers (Hofzumahaus et al., 2004), although due to their nature they are difficult to deploy for long periods of time, making either filter radiometers or spectral radiometers an attractive alternative (Bohn et al., 2008).

1.1 Techniques for the measurement of actinic flux density (F)

There are a range of radiometric techniques used for the determination of actinic flux, and the strengths of various detectors has been assessed by a field comparison experiment (Bohn et al., 2008). All these techniques relied on calibrations using reference light sources.

1.1.1 Estimating actinic flux density from irradiance measurements

The ideal viewing geometry for the determination of $F(\lambda)$ detects photons from all directions equally (all 4π steradian). For locations not over reflective surfaces like snow the upwelling radiation is relatively small, and so most measurements of $F(\lambda)$ are made viewing down-welling radiation only (e.g., Junkermann et al., 1989).

Most quantitative UV observations measure global irradiance (E) (the energy striking a horizontal plane), and so there have been a number of attempts to convert global irradiance into actinic flux (Kazadzis et al., 2004; Kylling et al., 2003; McKenzie et al., 2002; Schallhart et al., 2004; Webb et al., 2002).

If it is assumed that there is no upwelling radiation (surface albedo = 0), the actinic flux is given by

$$F = F_0 + F_{\downarrow} \tag{3}$$

where F_0 is the direct actinic flux density and $F_{\downarrow}$ is the diffuse component. Similarly, the global irradiance (E) is given by

$$E = \mu E_0 + E_{\downarrow} \tag{4}$$

where E_0 is now the direct beam irradiance, $\mu = \cos\theta$ where θ is the solar zenith angle and $E_{\downarrow}$ is the diffuse irradiance. As $E_0 = F_0$, it is now possible to simply write

$$F = \alpha E_{\downarrow} + E_0 = \alpha(E - E_0) + E_0 \tag{5}$$

where α is the ratio of the diffuse actinic flux density to diffuse irradiance. If the diffuse irradiance is not measured, equation (5) can be rearranged into the following relationship suggested by Kazadzis et al. (2004).

$$\frac{F}{E} = \alpha + (1 - \alpha\mu)\frac{E_0}{E} \tag{6}$$

The ratio α needs to be determined at the wavelengths relevant for the $O(^1D)$ photolysis (McKenzie et al., 2002; Webb et al., 2002), and this will be discussed in Section 3.1.

Estimating the ratio of the direct beam to global irradiance (E_0/E) has been more difficult. Schallhart et al. (2004) have therefore used a semi-empirical method which parameterized the relationship (F/E) based on the ratio of observed irradiance to clear sky irradiance, where the clear sky irradiance is calculated. Using data from four locations they found their results gave better agreement between measured and calculated F (7%, 2σ) than that reported using equation 6 and no knowledge of the direct to global irradiance ratio (Kylling et al., 2003; Webb et al., 2002). Using global irradiance measurements combined with direct irradiance every 10 nm, Kazadzis et al. (2004) estimate an overall uncertainty of around 10% (1σ).

1.1.2 Wavelength Sensitivity of Measurements

Three types of measurement detector have typically been used; a filter radiometer, a scanning spectrometer or a diode array/ CCD detector equipped spectrometer system (Bohn et al., 2008; Hofzumahaus et al., 2004). Each approach has limitations. The filter radiometer measures at a fixed wavelength range, which needs then to be calibrated using the actual atmospheric ozone column and solar zenith angle factors (Bohn et al., 2004). The scanning spectrometer takes time to scan through the spectrum, rather than measuring at a fixed time, leading to measures that are "time-smeared" rather than "time-averaged". For the production of a short-lived species like

$O(^1D)$ this can lead to difficulties in comparing with other measurements. Finally, the diode array/CCD system needs to have well characterized stray-light corrections applied (Bohn et al., 2008; Hofzumahaus et al., 2004; Edwards and Monks, 2003).

1.2 Estimates of $J(O^1D)$ at Cape Grim

The Cape Grim Baseline Air Pollution Station ("Cape Grim"), (40°40' 56"S, 144°41' 18"E) is a site near the northwest tip of Tasmania that experiences periods of clean maritime air from the southern ocean. During two intensive measurement campaigns SOAPEX - 1 (1995) (Monks et al. (1998)) and SOAPEX - 2 (1999) (Creasey et al., 2003) filter radiometers have been deployed to measure $J(O^1D)$. During SOAPEX -2 the OH concentration was also measured. The measurements during the second campaign clearly demonstrated a simple link between $O(^1D)$ production and OH concentrations in clean atmosphere conditions (Creasey et al., 2003).

As part of the Cape Grim measurement program spectral UV-B irradiance (both global and diffuse) has been measured routinely. The purpose of this work is to use the spectral UV-B measurements to estimate for the period 2000 - 2005, to assess estimates of the photolysis rates and to then develop a climatology. In particular, the impact of clouds and ozone will be assessed.

2 Experimental setup

All UV-B irradiance measurements reported here have been made in the radiation enclosure at the Cape Grim Baseline Air Pollution Station. This is located some 300m north of the main building (Cainey et al., 2007). The location avoids the shadow of the telecommunication tower that is situated just to the north of the main building. The experimental details of the UV-B measurements and in-situ calibration technique have been reported elsewhere (Wilson and Forgan, 1995; Wilson, 2006, 2007). In brief, the system alternately measures global and diffuse irradiance with a scanning double monochromator (Optronics Laboratories OL752) known as SRAD. Diffuse irradiance is measured by shading the global diffuser with a small shading disk mounted on the elevation arm of a tracker (Wilson, 2006). The spectral scans are spaced at 5

- 10 minute intervals, depending upon the time of day. The instrument is calibrated at 342 nm using well characterized sunphotometer measurements of direct beam irradiance, and the other wavelengths calibrated using the Ratio-Langley technique (Wilson and Forgan, 1995). All this is referenced to a top of the atmosphere spectrum (Chance and Kurucz, 2010) which serves as the primary calibration of both wavelength and intensity. The optical input for the system was modified in October 1999, resulting in higher optical throughput (and hence better signal/ noise ratios) and a diffuser with a better cosine response. The focus of this work is therefore on the period after the change in diffuser.

It is worth noting that the cosine error of the diffuser is determined from the solar zenith angle dependence of the ratio of the SRAD direct beam irradiance to the sunphotometer. A correction for this variation can then be applied during the calibration.

The resulting database of measurements includes alternating estimates of global and diffuse irradiance at each wavelength and time. The determination of the components of the irradiance at a single time is based on interpolation of the (e.g. diffuse) measurements before and after the (e.g. global) measurement in question (Wilson and Forgan, 1995), and so the derived signals are an approximation of the value for the 10 - 20 minute period around the nominal measurement time.

The input diffusers was constructed from PTFE but was not temperature controlled. The phase change reported for this material at around 292K (Ylianttila and Schreder, 2005) is therefore a source of uncertainty in these measurements. This will also impact upon the calibration, so that this will be at least partially captured in the variability of the calibrations.

3 Methodology

3.1 Derivation of $J(\mathrm{O}^1D)$ production from UV-B measurements

As the Cape Grim UV data set includes both the diffuse and global irradiance, equation 5 can be used, as the direct beam irradiance can be derived from the difference between the global and diffuse (see equation 4). This leaves the determination of the ratio (α). For the wavelength

region of interest (300 - 330 nm), a value of 2.0 could be used, which is the value appropriate for isotropic radiation (McKenzie et al., 2002) and clear skies. In cloudy conditions α decreases to values typically around 1.7 - 1.8. The calculations have been carried out using both the clear sky estimate of α and a value of 1.73, typical of cloudy conditions (Kylling et al., 2003) . For the analysis here the values using the lower value for α have been used unless otherwise noted.

For the ozone absorption cross section ($\sigma\ (\lambda, T)$, equation 2) the measurements of Malicet et al. (1995) at 22 °C have been used, in conjunction with the temperature dependent O^1D quantum yield (Sander et al., 2006), derived using the hourly average air temperature measured at Cape Grim (as part of the meteorology program) (Cainey et al., 2007).

The uncertainty in these derived $J(O^1D)$ values have been estimated, with details given in the supplementary information. In brief, the irradiance measures are estimated to have an uncertainty (1σ) of 9 - 12%. The combined uncertainty of all terms is found to be around 25%.

The UV-B measurements span the region 298 - 335 nm, and this can lead to an underestimate of the photolysis rate. A study by Jaekel et al. (2006) found that cut-offs below 298 nm did not perturb the estimate of $J(O^1D)$ by more than 5%, with the maximum error at times of low column ozone and high sun. Test measurements using spectra measuring out to 340 nm found that including the region between 335 – 340 nm altered $J(O^1D)$ by less than 1%. There is no recommended quantum yield for O^1D above 340 nm (Sander et al., 2006). The estimates presented here will therefore be biased low by the limited wavelength coverage by typically less than 5%.

The calibration uncertainty of the measurements is estimated to be 5% based on the uncertainties in the top of the atmosphere spectrum used as the calibration (Chance and Kurucz, 2010), and the variability in the calibration observed from the multiple calibrations carried out during the 6 years, implying a total uncertainty of around 8% in F(λ). This does not include the impact of model assumptions including the assumption of isotropic diffuse irradiance.

3.2 Modeling $J(O^1D)$

In the analysis of data the model TUV version 5.0 has been used (Madronich and Flocke, 1997). One of the changes in this version of the model is the use of the same solar spectrum (Chance

and Kurucz, 2010) as that used for the calibration of SRAD. The calculations have been run at a range of solar zenith angles using an aerosol optical depth of 0.05 at 550 nm, a value typical of conditions at Cape Grim (Wilson and Forgan, 2002). Because the model uses the same spectral data (top of the atmosphere spectrum, ozone cross section, quantum yield) the agreement between measurements and model should be close to the uncertainty in F, which is estimated to be around 12% (Supplementary material).

4 Results and Discussion

4.1 Comparison of measured $J(\mathrm{O}^1D)$ with model estimates

The measurements can be compared with the clear sky calculations performed using TUV 5.0. The results of this are shown in Figure 1, where the experimental values have been estimated using a clear sky estimate for α and the cloudy value. It can be seen that for the data from both February 2000 (low column ozone) and October 2003 (high column ozone) there is good agreement between model and measurement (average deviation 2%) if the clear sky estimate of α is used. Differences at high sun are around 3%. Several days exist where the irradiance appears to vary smoothly but with differences of up to 10% at solar noon. While this could be due in part to the limited measurement range (Section 3.2), a calibration issue that occurs at these solar zenith angles, or due to clouds. The smooth change in $J(\mathrm{O}^1D)$ implies no clouds near the sun, but there can be clouds well away from the sun that are altering the observed photolysis rate. Without a measure of the cloud field it is hard to distinguish between these possibilities.

4.2 Annual Cycle in $J(\mathrm{O}^1D)$

The data collected for the period 2000 - 2005 are shown in Figure 2. The dataset comprises over 108,000 measurements. The gaps in the dataset represent times when the equipment failed.

The annual cycle is the dominant feature in this plot. To quantify this, monthly mean values have been calculated by sorting all data from a month into 24 hourly bins, and from these bins

producing an average daily cycle for each month. It is assumed that if no measurement is made in one of the 24 hourly bins during the month that the average is zero. The average of the 24 hourly averages is then calculated for each month in the 6 years. This method has been used to limit the impact of possible biases from collecting spectra at varying time intervals.

Despite the variability seen in the individual measurements (See Figure 2), the monthly averages are relatively stable (Figure 3, top panel). The lower panel of Figure 3 shows that for mid-summer and mid-winter the interannual variability in the monthly averages is 3-4%, with the increases in-between presumably driven by the rate of change of the solar zenith angle at mid-day, the factor also driving much of the observed annual cycle. The resultant average monthly $J(\mathrm{O}^1D)$ for Cape Grim is also presented in Table 1 along with the standard deviations.

Measurements of $J(\mathrm{O}^1D)$ have been reported for 2002 - 2006 in the eastern Mediterranean (Gerasopoulos et al., 2012). The interannual variability in the monthly mean maxiumum clear sky irradiance is of the order of 7 - 8%. This is comparable to the monthly relative standard deviation in all measurements at Cape Grim (9.2%). The two locations are very different, both in terms of aerosol loadings and cloudiness, so the similarity is not expected.

Earlier measurements of interannual variability of UV-B have been reported for Ushuaia in Argentina (Frederick et al., 2001). For global irradiance at 305 nm they found an interannual variability (standard deviation/ average) of around 25%. The variability in global irradiance could be expected to be bigger than that for $J(\mathrm{O}^1D)$ with the different dependence on the angle of incidence of radiation. The mean of the monthly relative standard deviation (9.2%) is indeed slightly lower than that observed for global UV-B irradiance (10.8%) as determined from the Cape Grim data. However, both are significantly less than reported from Argentina. This is presumably a reflection of the difference in climate, with Cape Grim routinely experiencing cloudy conditions.

To investigate any trend in the data both monthly trends for each month and trends as a function of season have been calculated. The most significant linear trend is in summer (Dec - Feb) (-1.7 ± 1.1 (std. dev.) %/year), but this is not significant at the 90% level. Satellite estimates of changes in irradiance at 305 nm due to stratospheric ozone and clouds at this latitude are 0.3-0.4%/ year (averaged over 1979 - 2008) (Herman, 2010). For the shorter period

measured here it is not possible to detect changes of that magnitude, and local effects on clouds could determine the magnitude (and sign) of the observed trend.

4.3 Ozone Column Dependence

The dependence of $J(\mathrm{O}^1D)$ on solar zenith angle has been determined by sorting all data into 5° bins, and the results are summarized in Figure 4. For this plot, zenith angles up to 82.5° have been included. All measurements have been adjusted to 1 a.u. (correction for the annual variation in the earth-sun distance, (Iqbal, 1983)). A few measurements made at solar zenith angles less than 17.5 degrees have been excluded as they represent a brief period in mid-summer. Included in the plot are $J(\mathrm{O}^1D)$ estimates calculated using the TUV model for cloud free conditions and an aerosol optical depth of 0.05. Calculations for two ozone column amounts are shown, 250 and 350 DU, which are typical seasonal maximum and minimum values observed in this location as derived from satellite measurements (TOMS) (http://toms.gsfc.nasa.gov/index_v8.html).

A significant fraction of the variability can be due to the differences in the ozone column during the year. To characterize the dependence, functions of the following form were fitted to the the measured $J(\mathrm{O}^1D)$ values.

$$J(O^1D) = \left(\sum_i A_i \exp(-B_i/\cos\theta) \right) . \left({}^{O_3^{sat}}\!/_{300} \right)^{-RAF} \tag{7}$$

where θ is the solar zenith angle, O_3^{sat} is the total ozone column retrieved from satellite for the measurement day, and A_i, B_i and RAF are fitted. RAF is the Radiation Amplification Factor to be determined (Micheletti et al., 2003). The results for the fit to the entire dataset using either one or two exponential terms ($i = 1$ or 2) are shown in table 2 and for one exponential term in Figure 4. Using two exponentials produces a slightly better fit, and both fits produce an RAF estimate in excellent agreement with calculations of 1.4 - 1.5 (McKenzie et al., 2011).

Using this derived ozone RAF the dataset was normalized to both 300 DU and 1 a.u. as shown in Figure 5. Given the large difference between the median and average values for the bins, a

second fit was performed to the median of the binned values of Figure 5, and the fits are also included in Table 2. For reference, the fits with two exponential terms, using all data and the medians is included in Figure 5. It should be noted that the increase in R^2 is due to the change in the nature of the data being fitted.

The removal of the variation due to changes in stratospheric ozone, as described by the satellite ozone measurements, reduces the interquartile variability by up to 20% as shown in Figure 6. The effect on high sun (small solar zenith angle) measurements is smaller, as this is only collected in mid-summer and so the ozone variability is small. At larger solar zenith angles (>50°) the percentage reduction diminishes also, presumably because, as the absolute intensity decreases other effects, including the impact of measurement uncertainty, become larger.

4.4 Cloud Impact

Clouds can both reduce and enhance solar radiation at the ground level. Figure 5 shows that the 99 $^{\text{th}}$ percentile value closely follows the clear-sky calculated value at solar zenith angles less than 50°. This could be an aretfact due to biases in the clear sky calculations or measurement. If real, this implies that approximately 1% of these measurements show an enhancement of radiation due to clouds, a phenomenon often observed (Calbo et al., 2005). The likelihood of this cloud enhancement appears to increase with increasing solar zenith angle with up to 25% of measurements showing an enhancement by 65°, presumably as a result of the changes in scattering geometry in the atmosphere. This could also be due to errors in the model or unidentified cosine errors. However, the question does arise as to whether such behaviour is consistent with known cloud impacts on radiation.

To assess the overall impact of clouds, the ratio of the median value to the calculated clear - sky value was determined (Figure 7). This shows that for solar zenith angles less than 70°the median is approximately 75% of the calculated clear sky value. From 20 - 70°the calculated impact of clouds on $J(\mathrm{O}^1D)$ increases by 5 - 6%, a trend also predicted in models of the cloud impact on UV irradiance (Lindfors and Arola, 2008).

The results for solar zenith angles greater than 70°suggest that clouds have a diminishing impact as the sun approaches the horizon, as noted at other locations (Mateos et al., 2014). This

can be a result of the increasing importance of scattered light under these conditions due to the longer atmospheric path for the direct beam. As scattered radiation has become more significant, it could be expected that clouds more readily enhance the observed radiation (Figure 5) to the point that their overall impact is small (Figure 7). It can be concluded that the behaviour shown in Figure 7 is consistent with other measures of cloud properties. However, both measurement uncertainties (smaller signals and variations in detector angular response) and modelling limitations could be playing a significant role. The enhancement in inter-quartile range, also shown in Figure 7, could also be due to a combination of cloud impact or measurement uncertainty.

Attempts to capture the cloud variability through independent observations have not been very successful. Measures such as visual observations and automatic sky cameras have not been implemented at Cape Grim. While sunphotometers make measurements during this period, they do not make measurements of cloud optical depth as has been used elsewhere (Anton et al., 2012). Longwave downward radiation (LDR) measurements have been used to estimate cloudiness (Marty and Philipona, 2000; Dürr and Philipona, 2004). The attraction of this measure is that LDR is relatively insensitive to the solar position, and so should be independent of the other factors influencing $J(\mathrm{O}^1D)$. An attempt at using LDR has been made using half-hourly long-wave radiation averaged values measured at Cape Grim (Wilson and Shinkfield, 2007) to derive the Clear-Sky Index (Marty and Philipona, 2000). In this case it was possible to produce a fit extending equation (8) with an additional term (Clear-Sky Index)$^{\alpha}$, where α is a fitted parameter. Fitting the entire dataset where LDR values were available returned a significant value for the exponent (-0.19 ± 0.01). However, the fit did not improve significantly, as measured by the adjusted R^2 (increases of ˜0.0005). The lack of improvement in the fit suggests that this is not a useful approach. This could be due to the insensitivity of long-wave radiation measures to higher-level clouds (Schade et al., 2009; Boers et al., 2010). However, cloud bases are often low at Cape Grim (800 - 1000m) as observed by LIDAR measurements, (Young, 2007) and so LDR should be a reasonable measure. It is more likely that the features of clouds that cause changes in the observed LDR are not simply related to those features which result in a significant reduction (or enhancement) of $J(\mathrm{O}^1D)$.

A dependence on aerosols has been identified in measurements of $J(\mathrm{O}^1D)$ in the eastern Mediterranean (Gerasopoulos et al., 2012) which could be part of the variation identified here as a cloud impact. However, the low aerosol optical depth (mean of 0.07 at 500 nm compared with 0.23 in the Meditteranean (Gerasopoulos et al., 2011) makes this a small effect, especially when compared to the very common cloud cover at Cape Grim.

4.5 Wider Relevance of the Observations

The atmospheric composition at Cape Grim is dependent on wind direction and clean or "baseline" conditions are defined by standard measures (Downey, 2007). The impact of the photolysis measured here on the chemical composition of the atmosphere will depend on whether the local atmosphere is clean or polluted. However, an analysis of the data presented here filtered for only those measurements collected under "baseline" conditions gives results not statistically different from those observed for the entire dataset. As the baseline selection process eliminates a significant fraction of the data, the variability does increase.

Another important question is how reliably the climatology measured here is representative of a larger region. Cape Grim, sitting on the coast could have a cloud environment different to locations out to sea and inland. A study of the global irradiance at a number of locations concluded that Cape Grim experienced cloud conditions similar to the southern ocean in this area (Bishop et al., 1997), Studies of the clouds above Cape Grim showed that the cloud base is typically above 800m, well above the station (Young, 2007) and a study of rainfall has shown that while rainfall varies when moving inland it is reasonably constant along the coast (Jasper and Downey, 1991). The ISCCP dataset (http://isccp.giss.nasa.gov/index.html) shows that cloud amount at this latitude band over the oceans is 80 - 90%, with little dependence on longitude and without an obvious trend over the period 1984 - 2008. Therefore, the cloud impacts observed at Cape Grim should be representative of the marine environment at these latitudes.

Modelling studies (Liu et al., 2006) calculated that the impact of clouds on $J(\mathrm{O}^1D)$ is around 8% averaged throughout the troposphere, but that ground level impacts are larger, of the order of -20%. The data presented here shows an impact of clouds on $J(\mathrm{O}^1D)$ consistent with that estimate. The reduction in $J(\mathrm{O}^1D)$ is half that often observed for global UV irradiance at 80

- 90 % cloud cover, underlining the relative insensitivity of actinic flux to clouds (Calbo et al., 2005). This is a result of the relative importance of diffuse radiation to the photolysis rate, and the limited impact of clouds on total diffuse irradiance (Blumthaler et al., 1994).

The results of this study permit the prediction of $J(\mathrm{O}^1D)$ in the current climate. The impact of stratospheric ozone recovery should be well described by our current understanding. However, it would be useful to estimate the likely impact of future changes in cloud properties on $J(\mathrm{O}^1D)$. With the reasonable agreement between models and observations seen at Cape Grim there can be some confidence in their predictions. For the maritime environment investigated here the overall impact of clouds is relatively small (15 - 20%) given the 80-90 % cloud cover. Any future climate changes would need to change the frequency of clouds significantly to alter $J(\mathrm{O}^1D)$ greatly. Other changes, such as a change in cloud optical depth may be more significant. Verifying any such changes in $J(\mathrm{O}^1D)$ will require ongoing observations.

5 Conclusions

conclusionsSix years of estimates of $J(\mathrm{O}^1D)$ are presented for a clean southern hemisphere marine site. The impact of solar zenith angle and total column ozone can be clearly seen and quantified and the stratospheric ozone dependence is in good agreement with radiation model estimates. The impact of clouds can also be characterized, with bounds on the impact of clouds determined as a function of solar zenith angle. However, attempts at modelling the impact of clouds using independent radiation measurements (Longwave Downward Radiation) produced fits that did not significantly improve the quality of the model. So while the impact of clouds can be quantified, a good proxy for this has proven elusive.

Acknowledgements. This work would not be possible without the ongoing dedication and support of the staff at the Cape Grim Baseline Air Pollution Station and the financial support provided for work at Cape Grim by the Bureau of Meteorology. The inspiration of the other scientists involved in the Cape Grim programme is also gratefully acknowledged. The detailed and constructive comments from the referees have significantly improved this paper.

References

references

Anton, M., Alados-Arboledas, L., Guerrero-Rascado, J. L., Costa, M. J., Chiu, J. C., and Olmo, F. J.: Experimental and modeled UV erythemal irradiance under overcast conditions: the role of cloud optical depth, Atmospheric Chemistry and Physics, 12, 11 723–11 732, 2012.

Bishop, J. K. B., Rossow, W. B., and Dutton, E. G.: Surface solar irradiance from the International Satellite Cloud Climatology Project 1983 - 1991, Journal of Geophysical Research, 102, 6883–6910, doi:http://dx.doi.org/10.1029/96jd0386510.1029/96jd03865, 1997.

Blumthaler, M., Ambach, W., and Salzgeber, M.: Effects Of Cloudiness On Global and Diffuse UV Irradiance In a High-Mountain Area, Theoretical & Applied Climatology, 50, 23–30, 1994.

Boers, R., de Haij, M. J., Wauben, W. M. F., Baltink, H. K., van Ulft, L. H., Savenije, M., and Long, C. N.: Optimized fractional cloudiness determination from five ground-based remote sensing techniques, Journal of Geophysical Research, 115, doi:http://dx.doi.org/10.1029/2010jd01466110.1029/2010jd014661, 2010.

Bohn, B., Kraus, A., Muller, M., and Hofzumahaus, A.: Measurement of atmospheric $O_3 \rightarrow O(^1D)$ photolysis frequencies using filterradiometry, Journal Of Geophysical Research-Atmospheres, 109, doi:http://dx.doi.org/10.1029/2003JD00431910.1029/2003JD004319, 2004.

Bohn, B., Corlett, G. K., Gillmann, M., Sanghavi, S., Stange, G., Tensing, E., Vrekoussis, M., Bloss, W. J., Clapp, L. J., Kortner, M., Dorn, H.-P., Monks, P. S., Platt, U., Plass-Dülmer, C., Mihalopoulos, N., Heard, D. E., Clemitshaw, K. C., Meixner, F. X., Prevot, A. S. H., and Schmitt, R.: Photolysis frequency measurement techniques: results of a comparison within the ACCENT project, Atmos. Chem. Phys., 8, 5373 – 5391, 2008.

Cainey, J., Derek, N., and Krummel, P., eds.: Baseline Atmospheric Program 2005 - 2006, Australian Bureau of Meteorology and CSIRO Marine and Atmospheric Research, Melbourne, 2007.

Calbo, J., Pages, D., and Gonzalez, J. A.: Empirical studies of cloud effects on UV radiation: A review, Reviews of Geophysics, 43, doi:http://dx.doi.org/10.1029/2004rg00015510.1029/2004rg000155, 2005.

Chance, K. and Kurucz, R. L.: An improved high-resolution solar reference spectrum for earth's atmosphere measurements in the ultraviolet, visible, and near infrared, Journal of Quantitative Spectroscopy and Radiative Transfer, 111, 1289–1295, doi:http://dx.doi.org/10.1016/j.jqsrt.2010.01.03610.1016/j.jqsrt.2010.01.036, 2010.

Creasey, D. J., Evans, G. E., Heard, D. E., and Lee, J. D.: Measurements of OH and HO_2 concentrations in the Southern Ocean marine boundary layer, Journal of Geophysical Research, 108, 4475, doi:http://dx.doi.org/10.1029/2002JD00320610.1029/2002JD003206, 2003.

Crutzen, P. J.: Photochemical Reactions Initiated By And Influencing Ozone In Unpolluted Tropospheric Air, Tellus, 26, 47–57, 1974.

Downey, A.: Meteorology/ Climatology 2005-2006, in: Baseline Atmospheric Program Australia 2005-2006, edited by Cainey, J., Derek, N., and Krummel, P., pp. 39–45, Australian Bureau of Meteorology and CSIRO Marine and Atmospheric Research, Melbourne, 2007.

Dürr, B. and Philipona, R.: Automatic cloud amount detection by surface longwave downward radiation measurements, Journal of Geophysical Research, 109, D05 201, doi:http://dx.doi.org/10.1029/2003JD00418210.1029/2003JD004182, 2004.

Edwards, G. D. and Monks, P. S.: Performance of a single-monochromator diode array spectroradiometer for the determination of actinic flux and atmospheric photolysis frequencies, Journal Of Geophysical Research-Atmospheres, 108, doi:http://dx.doi.org/10.1029/2002JD00284410.1029/2002JD002844, 2003.

Frederick, J. E., Manner, V. W., and Booth, C. R.: Interannual variability in solar ultraviolet irradiance over decadal time scales at latitude 55 deg South, Photochemistry and Photobiology, 74, 771–779, 2001.

Gerasopoulos, E., Amiridis, V., Kazadzis, S., Kokkalis, P., Eleftheratos, K., Andreae, M. O., Andreae, T. W., El-Askary, H., and Zerefos, C. S.: Three-year ground based measurements of aerosol optical depth over the Eastern Mediterranean: the urban environment of Athens, Atmospheric Chemistry and Physics, 11, 2145–2159, 2011.

Gerasopoulos, E., Kazadzis, S., Vrekoussis, M., Kouvarakis, G., Liakakou, E., Kouremeti, N., Giannadaki, D., Kanakidou, M., Bohn, B., and Mihalopoulos, N.: Factors affecting O3 and NO2 photolysis frequencies measured in the eastern Mediterranean during the five-year period 2002-2006, Journal of Geophysical Research, 117, n/a–n/a, 2012.

Heard, D. E. and Pilling, M. J.: Measurement of OH and HO_2 in the troposphere, Chemical Reviews, 103, 5163–5198, 2003.

Herman, J. R.: Use of an improved radiation amplification factor to estimate the effect of total ozone changes on action spectrum weighted irradiances and an instrument response function, Journal of Geophysical Research, 115, D23 119, doi:http://dx.doi.org/10.1029/2010jd01431710.1029/2010jd014317, 2010.

Hofzumahaus, A., Lefer, B. L., Monks, P. S., Hall, S. R., Kylling, A., Mayer, B., Shetter, R. E., Junkermann, W., Bais, A., Calvert, J. G., Cantrell, C. A., Madronich, S., Edwards, G. D., Kraus, A., Muller, M., Bohn, B., Schmitt, R., Johnston, P., McKenzie, R., Frost, G. J., Griffioen, E., Krol, M., Martin, T., Pfister, G., Roth, E. P., Ruggaber, A., Swartz, W. H., Lloyd, S. A., and Van Weele, M.: Photolysis frequency of O_3 to O(^{1}D): Measurements and modeling during the International Photolysis Frequency Measurement and Modeling Intercomparison (IPMMI), Journal of Geophysical Research, 109, D08S90, doi:http://dx.doi.org/10.1029/2003JD00433310.1029/2003JD004333, 2004.

Iqbal, M.: An introduction to Solar Radiation, Academic Press, Toronto, 1983.

Jaekel, E., Wendisch, M., and Lefer, B.: Parameterization of Ozone Photolysis Frequency in the Lower Troposphere Using Data from Photodiode Array Detector Spectrometers, Journal of Atmospheric Chemistry, 54, 67–87, doi:http://dx.doi.org/10.1007/s10874-006-9014-110.1007/s10874-006-9014-1, 2006.

Jasper, J. and Downey, A.: Towards a Cape Grim Climatology, in: Baseline Atmospheric Program Australia 1989, edited by Wilson, S. R. and Gras, J. L., pp. 38–46, Bureau of Meteorology and the CSIRO Division of Atmospheric Research, Melbourne, 1991.

Junkermann, W., Platt, U., and Volz-Thomas, A.: A photoelectric detector for the measurement of photolysis frequencies of ozone and other atmospheric molecules, Journal of Atmospheric Chemistry, 8, 203–227, 1989.

Kazadzis, S., Topaloglou, C., Bais, A. F., Blumthaler, M., Balis, D., Kazantzidis, A., and Schallhart, B.: Actinic flux and (O ^{1}D) photolysis frequencies retrieved from spectral measurements of irradiance at Thessaloniki, Greece, Atmospheric Chemistry And Physics, 4, 2215–2226, 2004.

Kylling, A., Webb, A. R., Bais, A., Blumthaler, M., Schmitt, R., Thiel, S., Kazantzidis, A., Kift, R., Misslbeck, M., Schallhart, B., Schreder, J., Topaloglou, C., Kazadzis, S., and Rimmer, J.: Actinic flux determination from measurements of irradiance, Journal of Geophysical Research, 108, 4506, doi:http://dx.doi.org/10.1029/2002JD00323610.1029/2002JD003236, 2003.

Lindfors, A. and Arola, A.: On the wavelength-dependent attenuation of UV radiation by clouds, Geophysical Research Letters, 35, L05 806, doi:http://dx.doi.org/10.1029/2007GL03257110.1029/2007GL032571, 2008.

Liu, H., Crawford, J. H., Pierce, R. B., Norris, P., Platnick, S. E., Chen, G., Logan, J. A., Yantosca, R. M., Evans, M. J., Kittaka, C., Feng, Y., and Tie, X.: Radiative effect of clouds on tropospheric chemistry in a global three-dimensional chemical transport model, Journal of Geophysical Research, 111, D20 303, doi:http://dx.doi.org/10.1029/2005JD00640310.1029/2005JD006403, 2006.

Madronich, S. and Flocke, S.: Theoretical estimation of biologically effective UV radiation at the Earth's surface, in: Solar Ultraviolet Radiation - Modeling, Measurements and Effects, edited by Zerefos, C. and Bais, A., vol. NATO ASI Subseries 1, Vol. 52, pp. 23–48, Springer-Verlag, Berlin, 1997.

Malicet, J., Daumont, D., Charbonnier, J., Parisse, C., Chakir, A., and Brion, J.: Ozone UV Spectroscopy .2. Absorption Cross-Sections and Temperature Dependence, Journal of Atmospheric Chemistry, 21, 263–273, 1995.

Marty, C. and Philipona, R.: The clear-sky index to separate clear-sky from cloudy-sky situations in climate research, Geophysical Research Letters, 27, 2649–2652, doi:http://dx.doi.org/10.1029/2000gl01174310.1029/2000gl011743, 2000.

Mateos, D., di Sarra, A., Bilbao, J., Meloni, D., Pace, G., de Miguel, A., and Casasanta, G.: Spectral attenuation of global and diffuse UV irradiance and actinic flux by clouds, Quarterly Journal of the Royal Meteorological Society, doi:http://dx.doi.org/10.1002/qj.234110.1002/qj.2341, 2014.

McKenzie, R., Johnston, P., Hofzumahaus, A., Kraus, A., Madronich, S., Cantrell, C., Calvert, J., and Shetter, R.: Relationship between photolysis frequencies derived from spectroscopic measurements of actinic fluxes and irradiances during the IPMMI campaign, Journal Of Geophysical Research-Atmospheres, 107, doi:http://dx.doi.org/10.1029/2001JD00060110.1029/2001JD000601, 2002.

McKenzie, R. L., Aucamp, P. J., Bais, A. F., Bjorn, L. O., Ilyas, M., and Madronich, S.: Ozone depletion and climate change: impacts on UV radiation, Photochemical and Photobiological Sciences, 10, 182–198, doi:http://dx.doi.org/10.1039/C0PP90034F10.1039/C0PP90034F, 2011.

Micheletti, M. I., Piacentini, R. D., and Madronich, S.: Sensitivity of biologically active UV radiation to stratospheric ozone changes: Effects of action spectrum shape and wavelength range, Photochemistry and Photobiology, 78, 456–461, 2003.

Monks, P. S., Carpenter, L. J., Penkett, S. A., Ayers, G. P., Gillett, R. W., Galbally, I. E., and Meyer, C. P.: Fundamental ozone photochemistry in the remote marine boundary layer: The SOAPEX experiment, measurement and theory, Atmospheric Environment, 32, 3647–3664, 1998.

Rohrer, F. and Berresheim, H.: Strong correlation between levels of tropospheric hydroxyl radicals and solar ultraviolet radiation, Nature, 442, 184–187, 2006.

Sander, S. P., Friedl, R. R., Golden, D. M., Kurylo, M. J., Moortgat, G. K., Keller-Rudek, H., Wine, P. H., Ravishankara, A. R., Kolb, C. E., Molina, M. J., Finlayson-Pitts, B. J., Huie, R. E., and Orkin, V. L.: Chemical Kinetics and Photochemical Data for Use in Atmospheric Studies, Evaluation Number 15, Report JPL Publication 06-2, Jet Propulsion Laboratory, 2006.

Schade, N. H., Macke, A., Sandmann, H., and Stick, C.: Total and partial cloud amount detection during summer 2005 at Westerland (Sylt, Germany), Atmos. Chem. Phys., 9, 1143–1150, doi:http://dx.doi.org/10.5194/acp-9-1143-200910.5194/acp-9-1143-2009, 2009.

Schallhart, B., Huber, A., and Blumthaler, M.: Semi-empirical method for the conversion of spectral UV global irradiance data into actinic flux, Atmospheric Environment, 38, 4341–4346, 2004.

Webb, A. R., Kift, R., Thiel, S., and Blumthaler, M.: An empirical method for the conversion of spectral UV irradiance measurements to actinic flux data, Atmospheric Environment, 36, 4397–4404, 2002.

Wilson, S. R.: The Cape Grim Scanning UV Spectrometer, in: Baseline Atmospheric Program (Australia) 2003-2004, edited by Cainey, J., Derek, N., and Krummel, P. B., pp. 9–16, Bureau of Meteorology/ CSIRO Atmospheric Research, Melbourne, 2006.

Wilson, S. R.: Effect of temperature on the Cape Grim UV-B records, in: Baseline Atmospheric Program (Australia) 2005 - 2006, edited by Cainey, J., Derek, N., and Krummel, P. B., pp. 25–30, Australian Bureau of Meteorology and CSIRO Marine and Atmospheric Research, Melbourne, 2007.

Wilson, S. R. and Forgan, B. W.: In Situ Calibration Technique for UV Spectral Radiometers, Applied Optics, 34, 5475–5484, 1995.

Wilson, S. R. and Forgan, B. W.: Aerosol optical depth at Cape Grim, Tasmania 1986-1999, Journal of Geophysical Research, 107, 4068, doi:http://dx.doi.org/10.1029/2001JD00039810.1029/2001JD000398, 2002.

Wilson, S. R. and Shinkfield, P.: Passive solar radiation, in: Baseline Atmospheric Program (Australia) 2005 - 2006, edited by Cainey, J., Derek, N., and Krummel, P. B., p. 98, Australian Bureau of Meteorology and CSIRO Marine and Atmospheric Research, Melbourne, 2007.

Ylianttila, L. and Schreder, J.: Temperature effects of PTFE diffusers, Optical Materials, 27, 1811–1814, doi:http://dx.doi.org/10.1016/j.optmat.2004.11.00810.1016/j.optmat.2004.11.008, 2005.

Young, S. A.: Interpretation of the MiniLIDAR data recorded at Cape Grim 1998 - 2000, in: Baseline Atmospheric Program Australia 2005 - 2006, edited by Cainey, J., Derek, N., and Krummel, P., pp. 15–24, Australian Bureau of Meteorology and CSIRO Marine and Atmospheric Research, Melbourne, 2007.

References

references

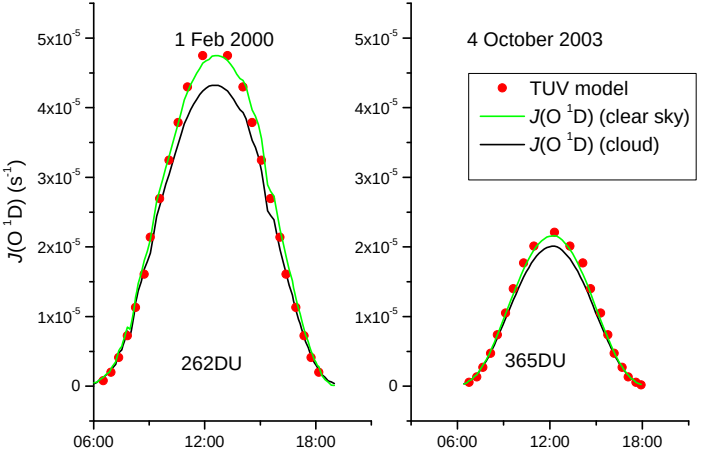

Fig. 1. Comparison of clear sky calculation values to measurements. Calculations have been performed using TUV 5.0 with the column ozone amount reported by satellite. $J(\mathrm{O}^1D)$ has been calculated using an α of 1.96 relevant to clear skies (green line) and 1.73 (cloudy - black line).
figure

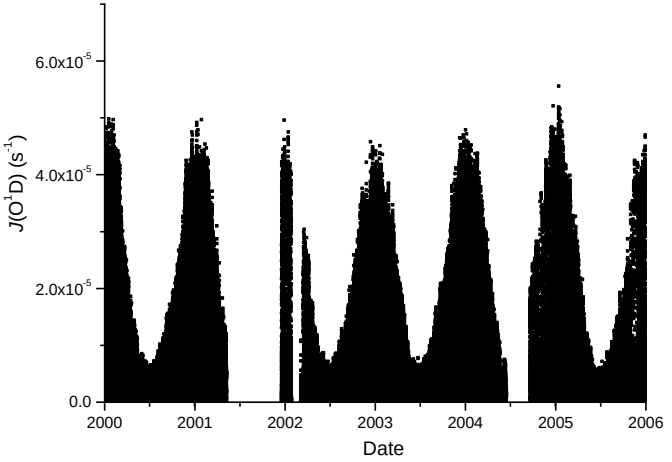

Fig. 2. Photolysis rate $J(\mathrm{O}^1D)$ observed at Cape Grim 2000 - 2005. Gaps in the data are due to instrument failure.

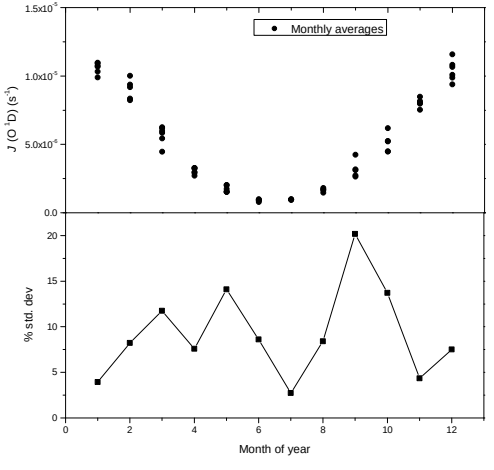

Fig. 3. Annual cycle of $J(\mathrm{O}^1D)$. The bottom panel shows the scatter in the monthly values as a percentage of the monthly mean.

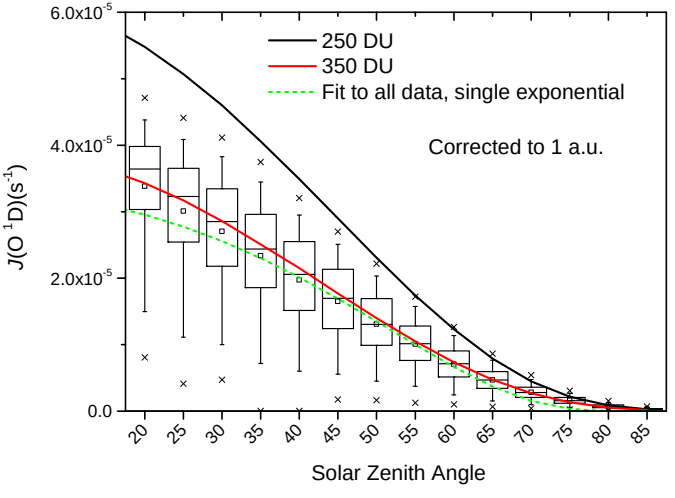

Fig. 4. Solar zenith angle dependence of $J(\mathrm{O}^1D)$. Crosses mark the 1 and 99 percentile. The boxes span 25/75%, the whiskers mark 10 and 90%, the central line indicates the median and the square the average value. The x-axis value is the central value of the 5° bin used. Included are the calculated $J(\mathrm{O}^1D)$ (TUV (V 5.0)) for ozone column amounts of 250 DU (February) (black solid line) and 350 DU (Sept) (red dashed line). The short-dashed green line is the fit to a single exponential term to all data.

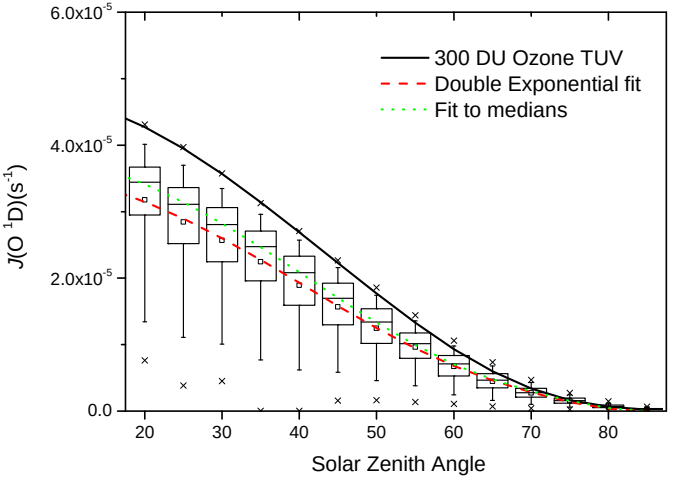

Fig. 5. Cape Grim measurements of $J(\mathrm{O}^1D)$ adjusted to a nominal 300 DU and 1 AU. The solid line is the calculated $J(\mathrm{O}^1D)$ for clear skies and 300 DU ozone column and an aerosol optical depth of 0.05 using TUV 5.0 (Madronich and Flocke, 1997). The two broken lines are the results of the fits to two exponential terms to either all data or the median value of each bin (See also table 2).

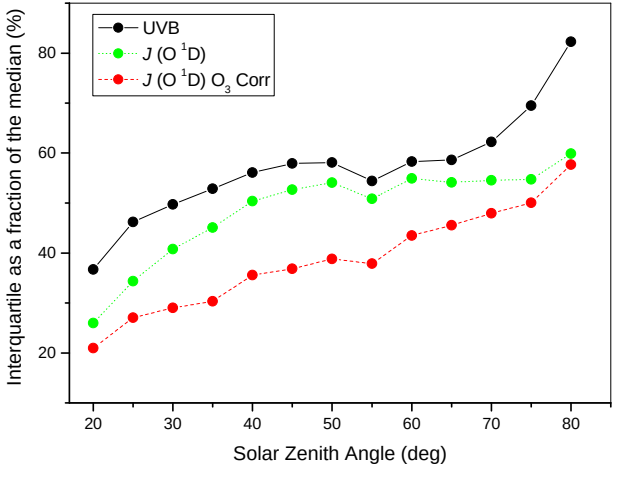

Fig. 6. The interquartile (75%-25%) difference as a percentage of the median value as a function of solar zenith angle. UVB is the global irradiance, and the other two terms are the derived photolysis rates, with the red curve measurements have been corrected to a constant column ozone amount.

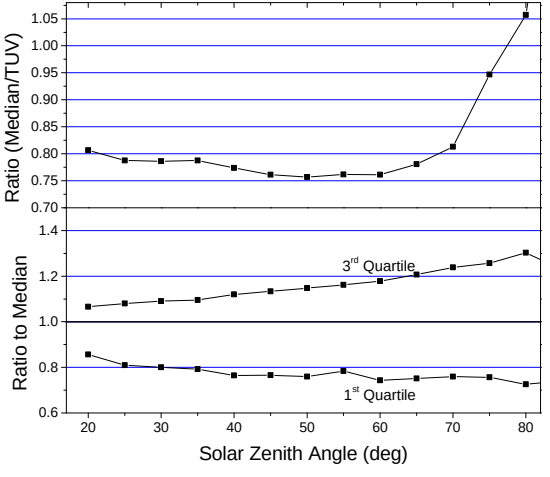

Fig. 7. Top panel shows the ratio of the median measured $J(\mathrm{O}^1D)$ to that from a calculation for clear skies. The bottom panel shows the spread in quartile values as a ratio to the median.

Table 1. Monthly mean photolysis rate $J(\mathrm{O}^1D)$. This is calculated using hourly averages for each of the 24 hours in the day.
table

Month	Mean (std. deviation) $\mathrm{s}^{-1} \times 10^{-6}$
1	10.59 (0.42)
2	9.02 (0.74)
3	5.69 (0.67)
4	3.06 (0..23)
5	1.72 (0.24)
6	0.90 (0.08)
7	0.96 (0.03)
8	1.65 (0.14)
9	3.18 (0.64)
10	5.12 (0.70)
11	8.03 (0.35)
12	10.40 (0.78)

Table 2. Results for fitting $J(\mathrm{O}^1D)$ with the form shown in equation 8. Brackets [] surround values that have been assumed in the fit. Uncertainties (in brackets) are standard errors in the last quoted figure of the fitted parameters. Units for A_1 and A_2 are s^{-1}. The "median fit" is a fit to the medians as shown in figure 6.

Fit	A_1 /10^{-4}	B_1	A_2 /10^{-5}	B_2	RAF	R^2
All data	1.608(7)	1.592(3)			1.403(9)	0.849
	4.6(1)	2.92(4)	2.4(1)	0.74(2)	1.426(9)	0.857
Medians	2.2(2)	1.77(8)			[1.43]	0.993
	4.4(5)	2.7(1)	1.8(5)	0.64(9)	[1.43]	1.000

Manuscript prepared for Atmos. Chem. Phys.
with version 2014/07/29 7.12 Copernicus papers of the LaTeX class copernicus.cls.
Date: 27 October 2014

Error Estimates for *J(O ^{1}D)*

S.R. Wilson

Contents

1 Introduction

This document summarizes the error esimates for the Cape Grim measurements of *J(O ^{1}D)*. These measurements have been made using a spectrometer (SRAD) that takes alternate measurements of global and diffuse irradiance. The photolysis rate (*J*) being estimated is defined by:

$$J(O^1D) = \int \sigma(\lambda,T)\phi(\lambda,T)F(\lambda)d\lambda \quad (1)$$

An explanation of the symbols used is given in Table 1. In this expression, we need to come up with an estimate of the uncertainty in all 3 terms. These will be addressed individually below, starting with the actinic flux density (F). This is the term that is driven by the Cape Grim measurements.

Table 1. Symbols used in this work.

Symbol	Meaning
S_0	Direct beam signal from SRAD
$S_\downarrow$	diffuse signal from SRAD
S	global signal from SRAD
θ	solar zenith angle
$F(\lambda)$	spectral actinic flux density
$\sigma(\lambda, T)$	ozone absorption cross section
$\phi(\lambda, T)$	quantum yield for (O ^{1D}) production
λ_r	Wavelength at which the reference sunphotometer operates
$c(\lambda_r, \theta)$	calibration for the direct beam irradiance atλ_r
$f(\theta)$	variation in instrument sensitivity

Section 2.1 summarises the calibration method and how F is derived from measurements. More details can be found on the calibration in Wilson and Forgan (1995). Section 2.2 then looks at the uncertainties in the determination of the irradiance, which is then combined to determine F. The final section then comments on the integration of this term with the other components needed to determine J.

2 Actinic Flux Density Estimate (F)

2.1 Theory

In summary, (F) is determined from the global signal S_0 and diffuse signal $S_\downarrow$, measured alternately and results interpolated to provide time coincidence :

$$S_0(\lambda) = (S(\lambda) - S_\downarrow(\lambda))/cos(\theta) \tag{2}$$

At the wavelength of a sunphotometer (λ_r) this value can then be calibrated by a factor $c(\lambda_r, \theta)$ $(V/(Wm^{-2}nm^{-1})$ derived from a calibrated sunphotometer measurement of direct beam irradiance at a wavelength λ_r $(E_{dir}(\lambda))$ collected at the same time as SRAD (solar zenith angle θ) :

$$c(\lambda_r, \theta) = (S_{dir}(\lambda_r, \theta)/(E_{dir}(\lambda_r, \theta)) \tag{3}$$

The calibration will be assumed to be separable into two factors, with $f(\theta)$ encompassing the variation in calibration due to an imperfect cosine response:

$$c(\lambda_r, \theta) = c(\lambda_r) * f(\theta) \tag{4}$$

At other wavelengths the relative calibration $c_{RL}(\lambda)$ is determined using the Ratio-Langley method Wilson and Forgan (1995). This determines the ratio of the top of the atmosphere instrument signals:

$$c_{RL}(\lambda) = {S_{dir}}^0(\lambda)/{S_{dir}}^0(\lambda_r) \tag{5}$$

So

$$c(\lambda) = c_{RL}(\lambda) * c(\lambda_r, \theta) * (E^0_{dir}(\lambda_r)/E^0_{dir}(\lambda_r)) \tag{6}$$

or

$$c(\lambda) = c_{RL}(\lambda) * c(\lambda_r) * f(\theta) * (E^0_{dir}(\lambda_r)/E^0_{dir}(\lambda_r)) \tag{7}$$

Presuming no azimuthal signal dependence, the diffuse irradiance at the sunphotometer wavelength can be derived assuming isotropic diffuse sky irradiance from:

$$S_{\downarrow}/E_{\downarrow}(\lambda_r) = \int sin(2\theta) * S_{dir}/E_{dir}(\lambda_r) d\theta \tag{8}$$

or

$$S_{\downarrow}/E_{\downarrow}(\lambda_r) = c(\lambda) \int sin(2\theta) * f(\theta)(\lambda_r) d\theta \tag{9}$$

Having calculated the direct and diffuse component, it is possible to determine the global irradiance from the direct and diffuse components:

$$E_0(\lambda) = E_{dir}(\lambda) * cos(\theta) + E_{\downarrow}(\lambda) \tag{10}$$

The Actinic flux density (F) can be calculated from these measured parameters using the relationship:

$$F(\lambda) = E_0(\lambda) + \alpha E_{\downarrow}(\lambda) \tag{11}$$

2.2 Derived uncertainty in F

The primary calibration reference for these measurements is the sunphotometer, which for these data is measuring at 342nm. This comparison provides both an estimate of the absolute calibration $c(\lambda_r)$ and an estimate of the measurement uncertainty associated with the global and diffuse irradiance. For Cape Grim, the uncertainty in the sunphotometer measurements needs to be less than 1%, as this corresponds to an uncertainty of 0.01 in aerosol optical depth. Aerosol optical depths at 342 nm have a median magnitude of around 0.06.

2.2.1 $c(\lambda_r)$

The uncertainty in the measurements (S) can be most readily estimated from the variation in $c(\lambda_r)$. This will contain the variability in both SRAD and the sunphotometer. The variation in this ratio will be assessed from the data 25/2/2003 - 31/12/2005. Prior to this time there were some changes in spectrometer configuration, altering $c(\lambda_r)$.

First, the solar zenith angle dependence needs to be considered. The ratio of spectrometer to sunphotometer can be plotted as a function of solar zenith angle (Figure 1) The medians show a maxiumum of 4 % deviation from the median at high and low solar zenith angles. The resultant binned medians can be fitted to a polynomial dependendent upon θ. Note that including this in the correction for the diffuse irradiance results in a change of 0.2 % .

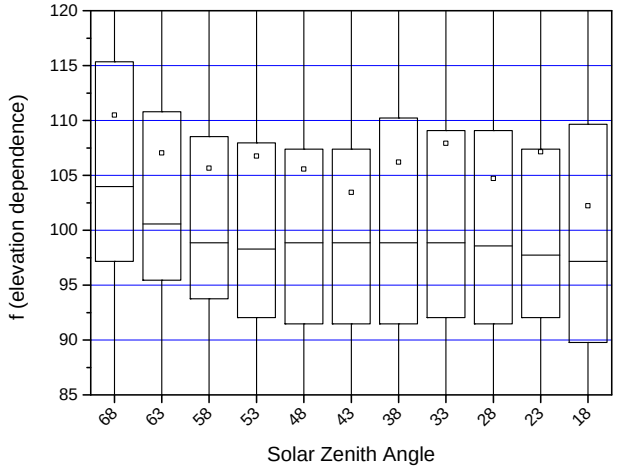

Figure 1. Ratio of derived direct beam irradiance to the sunphotometer signal, scaled by the median value for this period. Data from 25/2/2003 onwards, sorted by solar zenith angle.

Next, we need to look at $c(\lambda_r, \theta)$ which is directly derived from the two measurements. Assuming that the calibration factor for the period 2003 - 2005 is constant returns a median value for the calibration with a 95% confidence interval of less than 1% for the median value. The ratio of the signal from the two instruments displays a distribution is distinctly non-normal (using tests like the Shapiro-Wilk), so that care needs to be taken in estimating parameters. The median absolute deviation (MAD) of these ratio scaled to standard deviation equivalence, is 11.8 % of the median.

In order to assess the uncertainty in S and $S_{\downarrow}$ it has been assumed that they have a constant relative uncertainty. This is based on the ranging behaviour of the hardware and software. The relationship between the uncertainties in S and $S_{\downarrow}$ to the uncertainty in S_0 is non-linear. A trial and error method was therefore used, varying the assumed relative error in the diffuse and global irradiance for each measurement to derive a relative error in the direct beam signal. This was done for every

measurement where a comparison with the sun photometer was possible. The median value of the over 11,000 estimates of the uncertainty in S_0 has been compared to the scaled MAD derived above. On this basis it is estimated that the relative uncertainty in the original measurements is 5%.

2.2.2 $c^{rel}(\lambda)$

Typically during a year there are around 70 calibration periods (morning/ afternoon) that can be used for a ratio- Langley calibration. A similar number of clear mid-day periods are used for calibration below 305nm (Wilson, 2006). The mid-day calibrations are relative to 312.1 nm, using an ozone column amount derived from the B (305.5 nm/ 325.3 nm) and C (311.5 nm / 332.5 nm) wavelength pairs, where the calibrations for all wavelengths have been derived from the Ratio-Langly calibration. The calibration from the two types of Ratio-Langley method are joined at 312.1 nm.

Shown in Figure 2 are the average $c^{RL}(\lambda)$ and $c^{rel}(\lambda)$ for 2003. The smoothing applied to $c^{rel}(\lambda)$ is necessary as the lineshape of the instrument is presumably not well captured by the Gaussian assumed in deriving the top of the atmosphere irradiance. The derived $c^{rel}(\lambda)$ does change with time, and an annual average value has been used for each year. The ratio decreases throughout the measurement period, but the change in calibration between the years is less than 3 %. The % uncertainty in $c^{rel}(\lambda)$ is shown in Figure 3 for 2003.

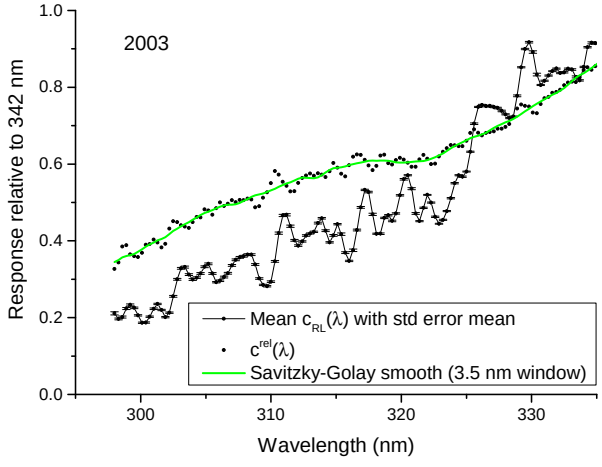

Figure 2. The Ratio-Langley calibration and the resultant relative sensitivity as a function of wavelength for 2003

The irradiance at the top of the atmosphere taken from Chance and Kurucz (2010). They ascribe an accuracy to their irradiances of better than 5%. This figure will be used for both irradiances. It is probable that the uncertainty in the irradiances are correlated, so that the true uncertainty in the irradiance ratio is less than this.

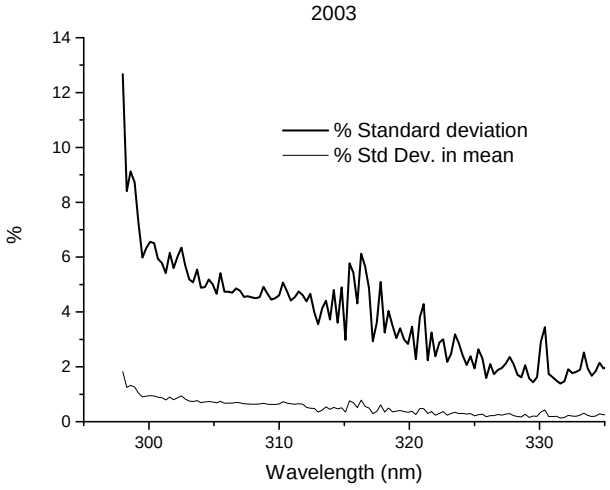

Figure 3. The standard deviation in the retrieved Ratio-Langley calibration for 2003.

2.2.3 $c(\lambda)$

The uncertainty in the calibration at any wavelength (λ) (see equation 7) can now be derived as the percentage uncertainties added in quadrature, giving an overall uncertainty of 14 % in the calibrated value, with the majority of this being driven by the estimation of measurement noise determined from the comparison of the direct beam measurements by SRAD and the sunphotometer. This estimate is only weakly dependent on wavelength as the dominant term is the uncertainty at λ_r.

2.3 Uncertainty in F

The uncertainty in F as derived from Equation 11 will contain the calibration uncertainty discussed above, and the uncertainty in α. Based on the work of Kylling et al. (2003) α should lie in a range 1.73 (cloud) - 1.96, where the values used in the calculation are for clear skies. This represents an uncertainty of the order of 10 %, implying an overall uncertainty of the order of 18 %.

From above, the uncertainty in E_0 is estimated to be approximately 12 %. The uncertainty in $\alpha E_{\downarrow}$ is very similar. Given that the two terms in equation (11) are not uncorrelated, it has been assumed that the uncertainty in F is comparable to the components (12 %).

2.4 Determination of $J(\mathrm{O}\,^1\mathrm{D})$

The combined uncertainty for the cross section and quantum yield for the production of O ^{1}D) from ozone is estimated to be 20 % by Sander et al. (2006).

The UV-B measurements span the region 298 - 335 nm, and this can lead to an underestimate of the photolysis rate. A study by Jaekel et al. (2006) found that cut-offs below 298 nm did not perturb

the estimate of $J(O^1D)$ by more than 5%, with the maximum error at times of low column ozone and high sun. Test measurements using spectra measuring out to 340 nm found that including the region between 335 – 340 nm altered $J(O^1D)$ by less than 1%. There is no recommended quantum yield for (O^1D) above 340 nm Sander et al. (2006). The estimates presented here will therefore be biased low by the limited wavelength coverage by typically less than 5%.

The resultant errors are summaries in Table 2. It should be noted that this does not include any estimate of the impact of model assumptions including the assumption of isotropic diffuse irradiance.

For comparison with the model TUV 5.0 (Madronich and Flocke, 1997) some of the uncertainties are common, as the same spectral data are used. Therefore the relevant uncertainty in comparing with the calculation is close to the uncertainty listed for F.

Table 2. Error estimates for the determination of $J(O^1D)$ from global and diffuse irradiance measurements using SRAD.

Error source	% uncertainty
Ref wavelength calibration at 342 nm	1
Uncertainty in global and diffuse	5
Ratio Langley relative calibration at 300 nm	1
Top of the atmosphere spectrum	7
α estimate	10
F determination	12
O_3 cross section/ (O ^{1}D) quantum yield	20
Combined error	23

References

Chance, K. and Kurucz, R. L.: An improved high-resolution solar reference spectrum for earth's atmosphere measurements in the ultraviolet, visible, and near infrared, Journal of Quantitative Spectroscopy and Radiative Transfer, 111, 1289–1295, doi:10.1016/j.jqsrt.2010.01.036, 2010.

Jaekel, E., Wendisch, M., and Lefer, B.: Parameterization of Ozone Photolysis Frequency in the Lower Troposphere Using Data from Photodiode Array Detector Spectrometers, Journal of Atmospheric Chemistry, 54, 67–87, doi:10.1007/s10874-006-9014-1, 2006.

Kylling, A., Webb, A. R., Bais, A., Blumthaler, M., Schmitt, R., Thiel, S., Kazantzidis, A., Kift, R., Misslbeck, M., Schallhart, B., Schreder, J., Topaloglou, C., Kazadzis, S., and Rimmer, J.: Actinic flux determination from measurements of irradiance, Journal of Geophysical Research, 108, 4506, doi:10.1029/2002JD003236, 2003.

Madronich, S. and Flocke, S.: Theoretical estimation of biologically effective UV radiation at the Earth's surface, vol. NATO ASI Subseries 1, Vol. 52, pp. 23–48, Springer-Verlag, Berlin, 1997.

Sander, S. P., Finlayson-Pitts, B. J., Friedl, R. R., Golden, D. M., Huie, R. E., Keller-Rudek, H., Kolb, C. E., Kurylo, M. J., Molina, M. J., Moortgat, G. K., Orkin, V. L., Ravishankara, A. R., and Wine, P. H.: Chemical Kinetics and Photochemical Data for Use in Atmospheric Studies, Evaluation Number 15, Report JPL Publication 06-2, Jet Propulsion Laboratory, 2006.

Wilson, S. R.: The Cape Grim Scanning UV Spectrometer, pp. 9–16, Bureau of Meteorology/ CSIRO Atmospheric Research, Melbourne, 2006.

Wilson, S. R. and Forgan, B. W.: In Situ Calibration Technique for UV Spectral Radiometers, Applied Optics, 34, 5475–5484, 1995.